Temperature-dependent electronic structure in a higher-order topological insulator candidate $EuIn_2As_2$

Sabin Regmi,[1] M. Mofazzel Hosen,[1] Barun Ghosh,[2] Bahadur Singh,[3,4] Gyanendra Dhakal,[1] Christopher Sims,[1] Baokai Wang,[3] Firoza Kabir,[1] Klauss Dimitri,[1] Yangyang Liu,[1] Amit Agarwal,[2] Hsin Lin,[5] Dariusz Kaczorowski,[6] Arun Bansil,[3] and Madhab Neupane[1,*]

[1]*Department of Physics, University of Central Florida, Orlando, Florida 32816, USA*
[2]*Department of Physics, Indian Institute of Technology Kanpur, Kanpur 208016, India*
[3]*Department of Physics, Northeastern University, Boston, Massachusetts 02115, USA*
[4]*Department of Condensed Matter Physics and Materials Science, Tata Institute of Fundamental Research, Colaba, Mumbai 400005, India*
[5]*Institute of Physics, Academia Sinica, Taipei 11529, Taiwan*
[6]*Institute of Low Temperature and Structure Research, Polish Academy of Sciences, 50-950 Wrocław, Poland*

(Received 28 November 2019; accepted 5 October 2020; published 29 October 2020)

Higher-order topological insulators (HOTIs) have enticed enormous research interests owing to their novelty in supporting gapless states along the hinges of a crystal. Despite several theoretical predictions, enough experimental confirmation of the HOTI state in crystalline solids is still lacking. It is shown that interplay between topology and magnetism can give rise to various magnetic topological states, including HOTI and axion insulator states. Here, using high-resolution angle-resolved photoemission spectroscopy combined with the first-principles calculations, we report a systematic study of the electronic structure and its evolution across the magnetic phase transition in $EuIn_2As_2$ which possesses an antiferromagnetic ground state below 16 K. Antiferromagnetic $EuIn_2As_2$ has been predicted to host both the axion insulator and the HOTI states. We directly observe the linearly dispersing holelike bands crossing the Fermi level and the change in their dispersion across the magnetic phase transition. Our paper points to $EuIn_2As_2$ as being a promising material for the exploration of interplay between topology and magnetism.

DOI: 10.1103/PhysRevB.102.165153

I. INTRODUCTION

The discovery of topological insulators (TIs) [1–4] has prompted intensive theoretical and experimental studies on realizing various topological states in quantum materials [5–9]. Owing to the bulk-boundary correspondence, the TIs support conducting surface states that lie within the gapped bulk electronic spectrum of the TIs. These surface states are spin polarized and disperse linearly with Dirac-cone energy dispersion. Constraints of the time-reversal symmetry protect the surface states from backscattering and localization in the presence of nonmagnetic perturbations thereby making TIs promising for low-power energy-efficient quantum electronic applications [10–12]. Recently, new types of topological insulating materials have come on the scene, which do not exhibit the usual bulk-boundary correspondence. They, dubbed as higher-order topological insulators (HOTIs) [13–15], possess bulk-surface-hinge correspondence where both the bulk and the surface states are gapped and the topology of the bulk bands supports gapless states along the hinges of the material. In HOTIs, the surfaces adjoining the hinges are required to be in different topological classes [16].

Topological states in HOTIs are protected by spatial symmetries, such as mirror, rotational, inversion, among others [14–18]. These states have been shown to exist in electronic circuits [19] as well as in photonic and phononic systems [20,21]. Recent work has reported the discovery of HOTI state in crystalline Bi via scanning-tunneling spectroscopy and Josephson interferometry aided by first-principles calculations [22]. Although HOTI states have been predicted in $EuIn_2As_2$ [23], Sm-doped Bi_2Se_3 [24], and other materials [15,25–28], their systematic momentum-resolved spectroscopic exploration is still lacking. The interplay between magnetism and topology is known to generate a variety of topological states including axion insulators [23,29,30], antiferromagnetic TIs [31–35], and magnetic topological states [36–40]. However, the experimental exploration of such states is held back due to limited availability of candidate magnetic materials with nontrivial band structures.

In this paper, by using high-resolution angle-resolved photoemission spectroscopy (ARPES) combined with parallel first-principles calculations, we systematically study the electronic properties of antiferromagnetic $EuIn_2As_2$, which is predicted to exhibit HOTI and axion insulator states. Our first-principles calculations reveal that $EuIn_2As_2$ exhibits an axion insulator state in both the AFM-B phase in which the magnetic moments lie *in plane* and the AFM-C phase in which the magnetic moments lie *out of plane*. Our experimental results show the evolution of the band structure in the vicinity of the Fermi level across the magnetic transition temperature. Our transport measurements find a metallic behavior over the

*Corresponding author: Madhab.Neupane@ucf.edu

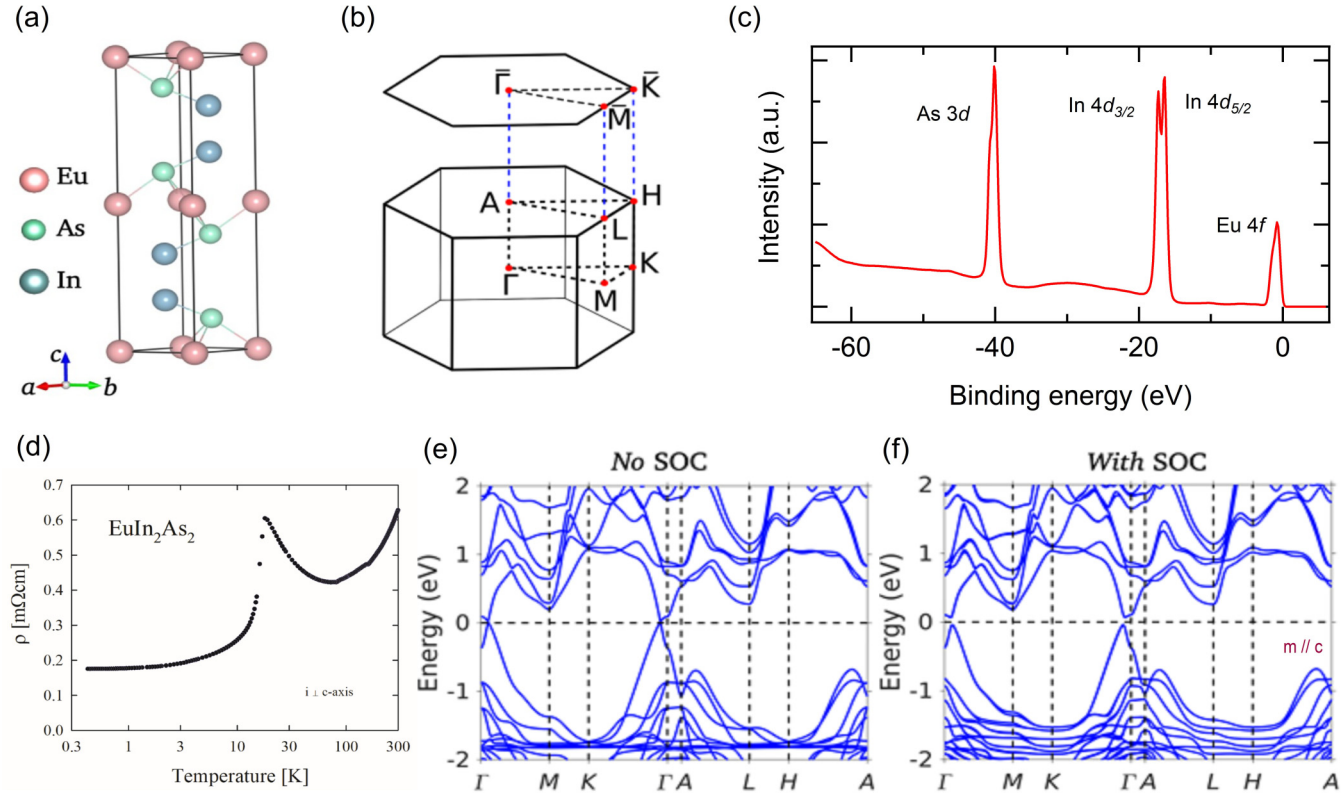

FIG. 1. Crystal structure and sample characterization of $EuIn_2As_2$. (a) Crystal structure of $EuIn_2As_2$. Red, seagreen, and cadetblue balls identify Eu, As, and In atoms, respectively. (b) Bulk and (001) surface Brillouin zones. High-symmetry points are marked. (c) Core-level photoemission spectrum with characteristic peaks of Eu $4f$, In $4d$, and As $3d$ orbitals. (d) Zero-field resistivity as a function of temperature. Bulk band structure (e) without and (f) with spin-orbit coupling.

entire temperature range investigated except at temperatures slightly higher than the antiferromagnetic transition temperature where Kondo-type behavior is observed. Our paper, thus, suggests that $EuIn_2As_2$ is a promising material for exploring interplay of topology and magnetism.

II. EXPERIMENTAL AND COMPUTATIONAL DETAILS

Single crystals of $EuIn_2As_2$ were grown by using the flux method [41]. We examined their chemical composition and crystal structure by energy-dispersive x-ray spectroscopy and single-crystal x-ray diffraction, respectively (see Supplemental Material (SM) for details [42]). Electrical behavior of $EuIn_2As_2$ was investigated as described in the SM [42]. ARPES measurements were performed at the Advanced Light Source (ALS), Berkeley on Beamline 10.0.1 equipped with a high-efficiency R4000 electron analyzer. The energy resolution was set better than 20 meV, and the angular resolution was set better than 0.2°. Samples were cleaved *in situ* and measured over 8–50 K in a vacuum better than 10^{-10} torr. Crystals were very stable for the typical measurement period of 20 h. In order to examine the nature of the states observed in $EuIn_2As_2$, the ARPES data were compared with the corresponding computed band dispersions projected onto the two-dimensional Brillouin zone (BZ). We performed the first-principles calculations within the framework of the density functional theory using the projector-augmented-wave pseudopotential method as implemented in the VASP software [43–45] (see the SM [42] for details).

III. RESULTS AND DISCUSSION

$EuIn_2As_2$ crystallizes in a hexagonal Bravais lattice with space-group $P6_3/mmc$ (No. 194) and lattice parameters $a = b = 4.207$ and $c = 17.889$ Å [41,46] [see Fig. 1(a)]. The crystal structure is layered where Eu, In, and As atomic layers occupy Wyckoff positions $2a$ $(0, 0, 0)$, $4f$ $(\frac{1}{3}, \frac{2}{3}, 0.17155)$, and $4f$ $(\frac{1}{3}, \frac{2}{3}, 0.60706)$, respectively. The associated bulk and (001) surface BZs are shown in Fig. 1(b) with high-symmetry points marked. Figure 1(c) presents the core-level photoemission spectrum which clearly shows the presence of the characteristic peaks coming from Eu $4f$, In $4d$, and As $3d$ orbitals indicating the high quality of our $EuIn_2As_2$ crystals.

Another proof of the quality of the $EuIn_2As_2$ single crystals grown is made by means of electrical transport measurements performed with electrical current flowing within the hexagonal a-b plane [see Fig. 1(d)]. The compound is found to exhibit metallic conductivity with a fairly large room-temperature resistivity of about 630 $\mu\Omega$ cm, and its $\rho(T)$ forming a distinct sharp maximum at the antiferromagnetic phase transition at $T_N = 16$ K. In the ordered state, the resistivity smoothly decreases with decreasing temperature, which reflects gradual reduction in scattering conduction electrons on magnetic moments carried by the Eu^{2+} ions. At the lowest temperatures,

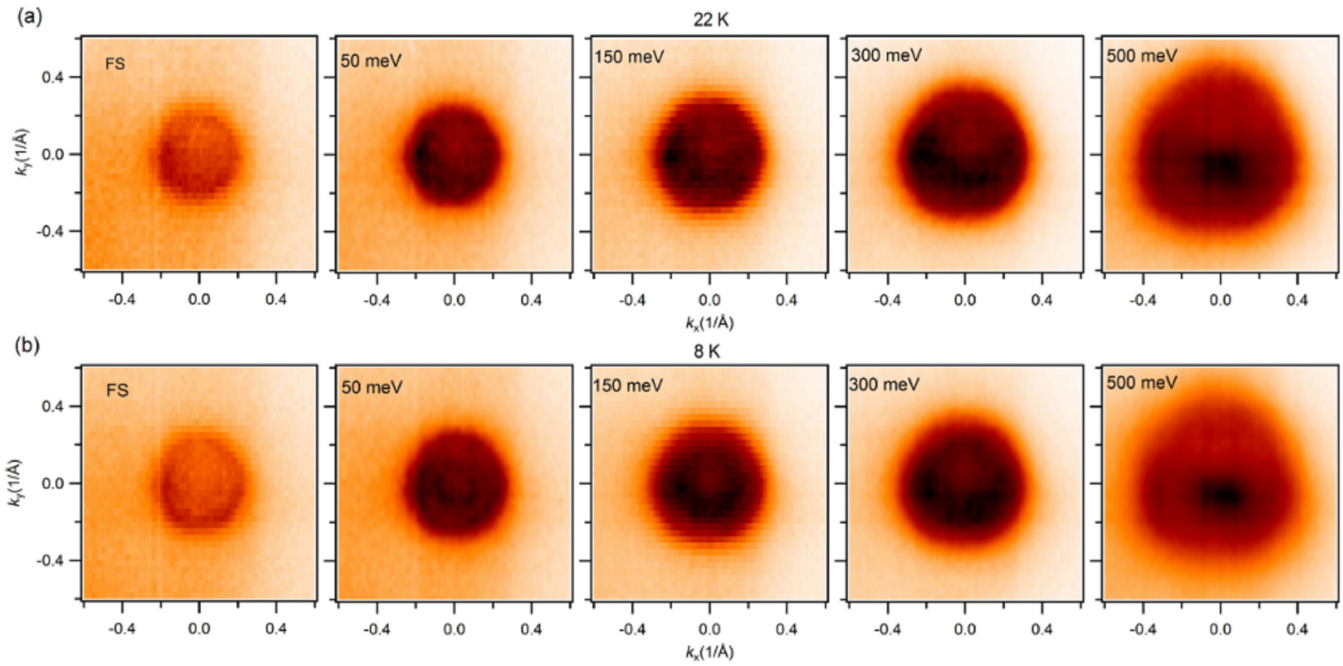

FIG. 2. Fermi surface map and constant energy contours of $EuIn_2As_2$. (a) Fermi surface (leftmost) and constant energy contours measured at a temperature of 22 K. (b) Same as (a) but measured at 8 K. The binding energy is marked on each panel. Data were collected at the ALS beamline 10.0.1 using a photon energy of 60 eV.

$\rho(T)$ makes a plateau, and the resistivity saturates at a residual value of about 180 $\mu\Omega$ cm observed near 0.4 K. Both the shape of $\rho(T)$ and the resistivity magnitude are in concert with the literature data [41,46].

The electric measurements show that $EuIn_2As_2$ exhibits an antiferromagnetic ground state. To gain insight into its electronic band topology, we present the calculated bulk band structure in Figs. 1(e) and 1(f). In the absence of spin-orbit coupling (SOC), the valence and conduction bands dip into each other to produce a band inversion with an inverted band gap of 0.46 eV at the Γ point [see Fig. 1(e)]. Although the band structure resembles band crossing features around the Γ-K and Γ-M directions, we find that the bands along the Γ-M direction are gapped whereas they are gapless and symmetry protected along the Γ-K direction [23]. After including SOC, all the band crossings are gapped, separating valence and conductions bands [Fig. 1(f)]. We consider two antiferromagnetic (AFM) configurations: AFM-B in which magnetic moments lie *in plane*, and AFM-C in which magnetic moments lie *out of plane* (see the SM for the comparison of bulk crystal and band structures of paramagnetic, AFM-B, and AFM-C phases [42]). The AFM-B and AFM-C states are nearly degenerate with an energy difference of less than 1 meV per unit cell in agreement with earlier theoretical results [23].

Since both AFM-B and AFM-C configurations are gapped with a band inversion, we determine their topological state by calculating the parity-based $\mathbb{Z}_4$ topological invariant [23,47–49], which is defined as

$$\mathbb{Z}_4 = \sum_{i=1}^{8} \sum_{n=1}^{N_{\rm occ}} \frac{1+\zeta_n(\Gamma_i)}{2} \bmod 4. \qquad (1)$$

Here, ζ_n (Γ_i) is the parity at the ith time-reversal invariant momenta point Γ_i for the nth band, and N_{occ} is the number of occupied bands. We find $\mathbb{Z}_4 = 2$ for both the AFM-B and the AFM-C configurations which indicate that $EuIn_2As_2$ is an axion insulator.

Although $\mathbb{Z}_4 = 2$ indicates that $EuIn_2As_2$ is an axion insulator, it can still be characterized based on the magnetic group symmetries. Specifically, the AFM-B phase supports two mirror planes $k_y = 0$ and $k_z = 0$ with a nonzero mirror Chern number, indicating a topological crystalline insulator phase. On the contrary, there is no such preserved mirror plane in the AFM-C phase, and, as a result, AFM-C realizes the HOTI state with $\mathbb{Z}_4 = 2$. We have also examined the paramagnetic state by freezing Eu f electrons and found the system to be a topological insulator with a nonzero $\mathbb{Z}_2$ invariant $(\nu_0; \nu_1\nu_2\nu_3) = (1; 000)$.

We now present our ARPES measured Fermi surface and constant energy contour results measured at different binding energies in both the paramagnetic and AFM phases in Fig. 2. The constant energy contours measured at 22 K are presented in Fig. 2(a), which shows their evolution with increasing the binding energy from zero (Fermi surface) to 500 meV. Figure 2(b) represents constant energy contours at various binding energies taken at 8 K (below the AFM transition temperature). One can resolve the circular energy pockets in both the paramagnetic and the AFM states. A careful inspection of constant energy contours reveals that an inner circular pocket appears in the AFM state, which is absent in the paramagnetic phase and can be well resolved at 50-meV binding energy. The absence of this extra feature in the paramagnetic phase is also confirmed by measurements at a temperature of 46 K (see the SM [42]). The size of this inner circular contour grows as one goes to higher binding energies, and it finally merges with the outer circular pocket at 300 meV, indicating the holelike nature of the associated states. At the higher binding energy of

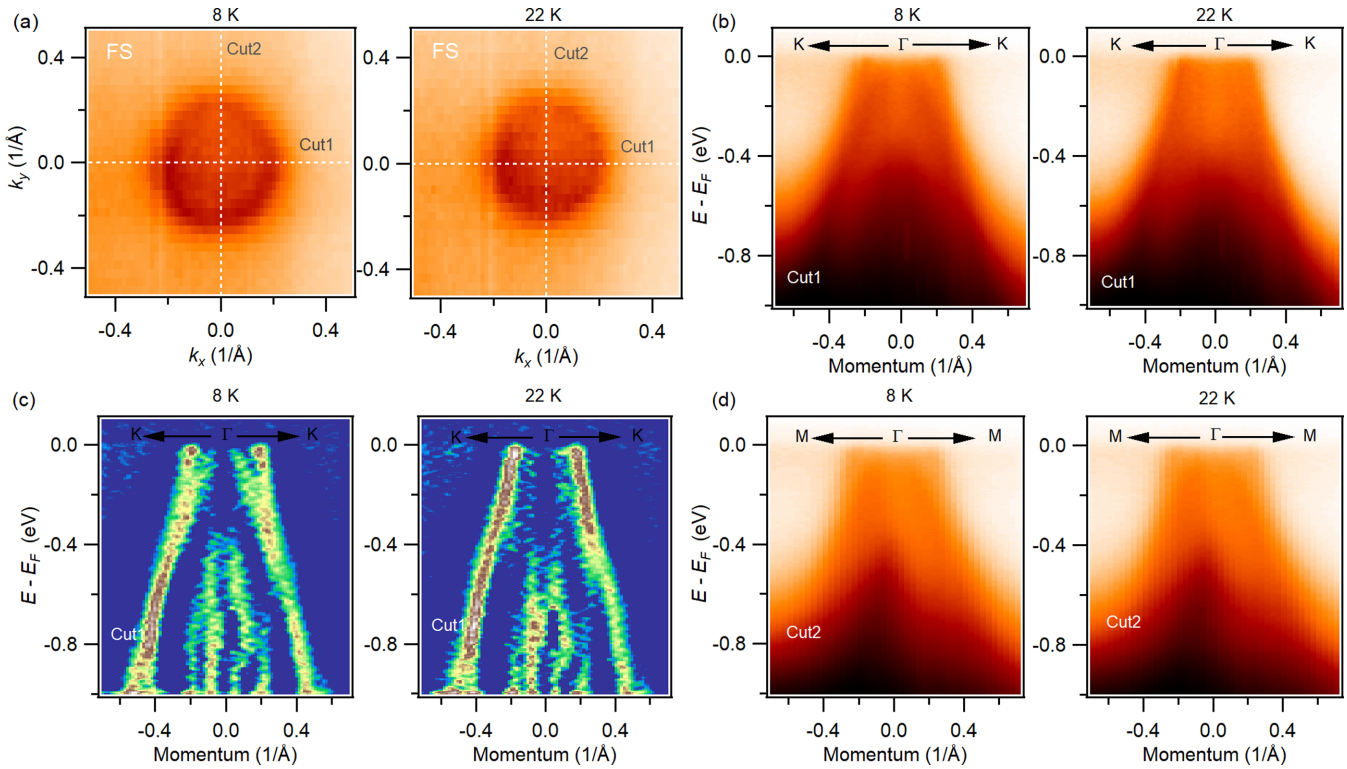

FIG. 3. Experimentally obtained electronic structure along various momentum directions. (a) Fermi-surface maps at different temperatures where the white dashed lines identify the cut directions along which the dispersion maps are taken. (b) Energy dispersion along the cut 1 direction (K-Γ-K) in (a). (c) Second derivative plot of dispersion maps in (b). (d) Energy dispersion along the cut 2 direction (M-Γ-M) in (a). Temperature is noted on each plot. All data were taken at the ALS beamline 10.0.1 using a photon energy of 60 eV.

500 meV, the inner circular contour in AFM phase vanishes and a new rectangular holelike bulk feature appears in both the paramagnetic and the AFM states, although the size of this rectangular pocket in the AFM phase is smaller than that in the paramagnetic phase.

Figure 3 presents the dispersion maps along different momentum directions in both the paramagnetic and the AFM phases. Figure 3(a) shows the Fermi surface at 8 K (left) and 22 K (right) where the white dashed lines represent the cut directions along which the dispersion maps are taken. The left panel in Fig. 3(b) shows the band dispersion along the cut 1 direction (K-Γ-K) at 8 K. The two linear holelike bands are clearly resolved near the Fermi level and extend well below the Fermi level up to ∼400-meV binding energy, consistent with the results for Fermi surface and constant energy contours in Fig. 2(b). The right panel in Fig. 3(b) shows the band dispersion along the K-Γ-K direction at 22 K. The holelike band can be seen crossing the Fermi level, but the second band near the Fermi level is absent. Absence of this second band in the paramagnetic phase is also confirmed by our measurements at 46 K (see the SM [42]). These results dictate that, although the outer holelike state with linear energy dispersion stays robust across the AFM phase transition, the inner band is sensitive to magnetism. These features are further resolved in the second derivative plots in Fig. 3(c). We present the energy dispersion measured along the cut 2 (M-Γ-M direction) in Fig. 3(d) where the extra feature cannot be well resolved.

To better illustrate the changes in electronic structure across the magnetic phase transition, we present the second derivative of the constant energy contours at 50-meV binding energy and the momentum distribution curves (MDCs) along the K-Γ-K direction in Fig. 4. The second derivative of the energy contour in Fig. 4(a) in the AFM state at 8 K clearly shows an inner feature, which is absent in the paramagnetic phase at 22 K in Fig. 4(b). Figure 4(c) shows the MDC plot along the K-Γ-K direction in the AFM phase. The two-peak feature near the Fermi level (see arrows marked on the figure) is seen to merge into a single peak as we go to higher binding energies. However, in the paramagnetic phase (Fig. 4(d), also see the SM [42]), we only see the single peak feature.

Splitting of the hole band in the magnetic state is also supported by our theoretical surface state calculations. In Fig. 5, we present (001) surface states obtained for As termination with a modified surface potential for the magnetic and nonmagnetic phases. In the paramagnetic phase [Fig. 5(c)], a doubly degenerate nontrivial hole band crosses the Fermi level with the nontrivial Dirac-cone state lying above it. Such an energy dispersion results in a single hole band at the Fermi level and at −50 meV [Fig. 5(f)] in reasonable agreement with our experimental results for $T > T_N$. Surface band structures below T_N in both the AFM-B and the AFM-C phases are shown in Figs. 5(a) and 5(b), respectively. The presence of magnetism uplifts the surface state degeneracy giving rise to two-hole bands. Notably, both the AFM-B and the AFM-C states give similar energy dispersion in the hole doped regime. However, the AFM-B phase realizes a gapless type-II Dirac-cone state whereas AFM-C yields a gapped surface state above the Fermi level consistent with the calculated bulk

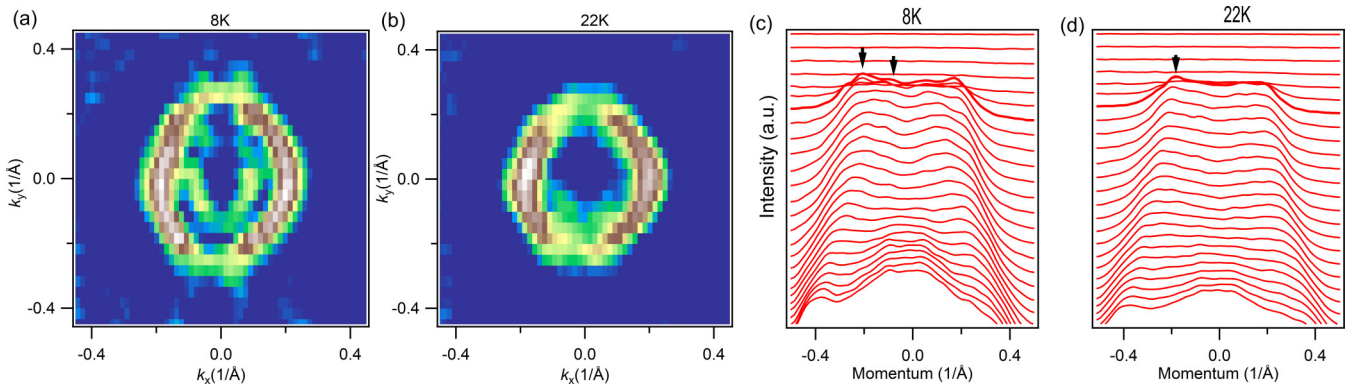

FIG. 4. Temperature-dependent electronic structure of $EuIn_2As_2$. (a) Second derivative plots of the constant energy contours at the binding energy of 50 meV in the AFM state at 8 K (left) and the paramagnetic state at 22 K (right). (b) MDCs in the vicinity of Fermi level along the K-Γ-K direction in the AFM state at 8 K (left) and paramagnetic state at 22 K (right). Changes in the energy dispersion across the AFM transition are resolved clearly.

invariants. Although both AFM-B and AFM-C energy dispersions are in agreement with the experiments in the hole-doped regime, the nature of states above the Fermi level is essential to identify the exact topological state of AFM $EuIn_2As_2$.

IV. CONCLUSION

Our paper explores the electronic structure of $EuIn_2As_2$ across the AFM transition by using temperature-dependent high-resolution ARPES along with parallel first-principles computation. In the paramagnetic phase, the two linearly dispersing degenerate holelike bands are found to cross the Fermi level with the Dirac point located above the Fermi level (see the SM [42] for the energy position of the Dirac point). As the temperature is lowered, $EuIn_2As_2$ transitions into the AFM state where doubly degenerate hole band splits in energy in the vicinity of the Fermi level. Combined with our first-principles bulk and surface-state computations, our experimental results point to the possibility that $EuIn_2As_2$ harbors a topological magnetic state. Since the Dirac point is located above the

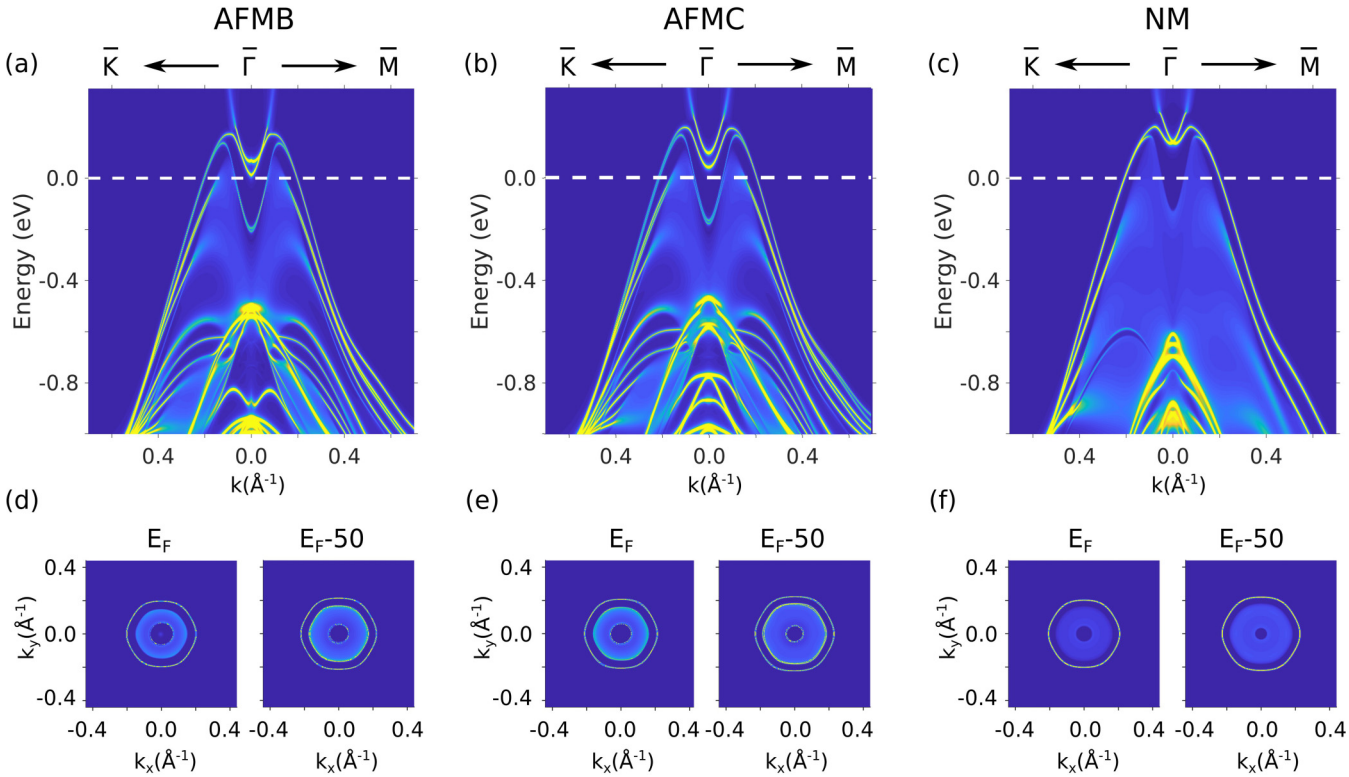

FIG. 5. The (001) surface band structure and the associated constant energy contours for the antiferromagnetic state with (a) and (d) in-plane (AFMB), (b) and (e) out-of-plane (AFMC) magnetic moments. (c) and (f) The (001) surface band structure and the related constant energy contours for the nonmagnetic (NM) state. A modified surface potential was used in these calculations. The Fermi level was shifted to improve comparison with the experimental results.

Fermi level, it can be tuned to the Fermi level via the electrical gating or chemical doping. Notably, transport measurements show a Kondo-type behavior at temperatures slightly above the magnetic transition temperature. Our paper suggests that $EuIn_2As_2$ could provide a promising new material platform for exploring topological magnetic states and their evolution from nonmagnetic states.

ACKNOWLEDGMENTS

M.N. was supported by the Air Force Office of Scientific Research under Award No. FA9550-17-1-0415 and the National Science Foundation (NSF) CAREER Award No. DMR-1847962. The work at Northeastern University was supported by the US Department of Energy (DOE), Office of Science, Basic Energy Sciences Grant No. DE-FG02-07ER46352, and benefited from Northeastern University's Advanced Scientific Computation Center (ASCC) and the NERSC supercomputing center through DOE Grant No. DE-AC02-05CH11231. B.G. acknowledges the CSIR for Senior Research Fellowship. The work at IIT Kanpur was benefited from the high-performance facilities of the computer center of IIT Kanpur. This research used resources of the Advanced Light Source (ALS), a US Department of Energy Office of ScienceUser Facility, under Contract No. DE-AC02-05CH11231. We thank S.-K. Mo for beamline assistance at the ALS, Lawrence Berkeley National Laboratory (LBNL).

[1] M. Z. Hasan and C. L. Kane, Rev. Mod. Phys. **82**, 3045 (2010).
[2] X.-L. Qi and S.-C. Zhang, Rev. Mod. Phys. **83**, 1057 (2011).
[3] M. Z. Hasan, S.-Y. Xu, and M. Neupane, in *Topological Insulators: Fundamentals and Perspectives*, edited by F. Ortmann, S. Roche, and S. O. Valenzuela (Wiley, Hoboken, NJ, 2015).
[4] A. Bansil, H. Lin, and T. Das, Rev. Mod. Phys. **88**, 021004 (2016).
[5] M. Neupane, S.-Y. Xu, R. Sankar, N. Alidoust, G. Bian, C. Liu, I. Belopolski, T.-R. Chang, H.-T. Jeng, H. Lin, A. Bansil, F. Chou, and M. Z. Hasan, Nat. Commun. **5**, 3786 (2014).
[6] S.-Y. Xu, I. Belopolski, N. Alidoust, M. Neupane, G. Bian, C. Zhang, R. Sankar, G. Chang, Z. Yuan, C.-C. Lee, S.-M. Huang, H. Zheng, J. Ma, D. S. Sanchez, B. Wang, A. Bansil, F. Chou, P. P. Shibayev, H. Lin, S. Jia, and M. Z. Hasan, Science **349**, 613 (2015).
[7] M. Neupane, I. Belopolski, M. M. Hosen, D. S. Sanchez, R. Sankar, M. Szlawska, S.-Y. Xu, K. Dimitri, N. Dhakal, P. Maldonado, P. M. Oppeneer, D. Kaczorowski, F. Chou, M. Z. Hasan, and T. Durakiewicz, Phys. Rev. B **93**, 201104(R) (2016).
[8] M. M. Hosen, K. Dimitri, A. K. Nandy, A. Aperis, R. Sankar, G. Dhakal, P. Maldonado, F. Kabir, C. Sims, F. Chou, D. Kaczorowski, T. Durakiewicz, P. M. Oppeneer, and M. Neupane, Nat. Commun. **9**, 3002 (2018).
[9] K. Dimitri, M. M. Hosen, G. Dhakal, H. Choi, F. Kabir, C. Sims, D. Kaczorowski, T. Durakiewicz, J.-X. Zhu, and M. Neupane, Phys. Rev. B **97**, 144514 (2018).
[10] S. A. Wolf, D. D. Awschalom, P. A. Buhrman, J. M. Daughton, M. L. von Molna Roukes, A. Y. Chtchelnakova, and D. M. Treger, Science **294**, 1488 (2001).
[11] X.-L. Qi, R. Li, J. Zang, and S.-C. Zhang, Science **323**, 1184 (2009).
[12] J. Linder, Y. Tanaka, T. Yokoyama, A. Sudbø, and N. Nagaosa, Phys. Rev. Lett. **104**, 067001 (2010).
[13] W. A. Benalcazar, B. A. Bernevig, and T. L. Hughes, Science **357**, 61 (2017).
[14] W. A. Benalcazar, B. A. Bernevig, and T. L. Hughes, Phys. Rev. B **96**, 245115 (2017).
[15] F. Schindler, A. M. Cook, M. G. Vergniory, Z. Wang, S. S. P. Parkin, B. A. Bernevig, and T. Neupert, Sci. Adv. **4**, eaat0346 (2018).
[16] J. Langbehn, Y. Peng, L. Trifunovic, F. von Oppen, and P. W. Brouwer, Phys. Rev. Lett. **119**, 246401 (2017).
[17] Z. Song, Z. Fang, and C. Fang, Phys. Rev. Lett. **119**, 246402 (2017).
[18] E. Khalaf, Phys. Rev. B **97**, 205136 (2018).
[19] S. Imhof, C. Berger, F. Bayer, J. Brehm, L. W. Molenkamp, T. Kiessling, F. Schindler, C. H. Lee, M. Greiter, T. Neupert, and R. Thomale, Nat. Phys. **14**, 925 (2018).
[20] C. W. Peterson, W. A. Benalcazar, T. L. Huges, and G. Bahl, Nature (London) **555**, 346 (2018).
[21] M. Serra-Garcia, V. Peri, R. Susstrunt, O. R. Bilal, T. Larsen, L. G. Villaneuva, and S. D. Huber, Nature (London) **555**, 342 (2018).
[22] F. Schindler, Z. Wang, M. G. Vergniory, A. M. Cook, A. Murani, S. Sengupta, A. Y. Kasumov, R. Deblock, S. Jeon, I. Drozdov, H. Bouchiat, S. Guéron, A. Yazdani, B. A. Bernevig, and T. Neupert, Nat. Phys. **14**, 918 (2018).
[23] Y. Xu, Z. Song, Z. Wang, H. Weng, and X. Dai, Phys. Rev. Lett. **122**, 256402 (2019).
[24] C. Yue, Y. Xu, Z. Song, H. Weng, Y.-M. Lu, C. Feng, and X. Dai, Nat. Phys. **15**, 577 (2019).
[25] M. Ezawa, Phys. Rev. Lett. **120**, 026801 (2018).
[26] M. Ezawa, Phys. Rev. B **98**, 045125 (2018).
[27] H. Xue, Y. Yang, F. Gao, Y. Chong, and B. Zhang, Nat. Mater. **18**, 108 (2019).
[28] R.-X. Zhang, F. Wu, and S. D. Sarma, Phys. Rev. Lett. **124**, 136407 (2020).
[29] N. Varnava and D. Vanderbilt, Phys. Rev. B **98**, 245117 (2018).
[30] D. Zhang, M. Shi, T. Zhu, D. Xing, H. Zhang, and J. Wang, Phys. Rev. Lett. **122**, 206401 (2019).
[31] M. M. Otrokov, I. I. Klimovskikh, H. Bentmann, D. Estyunin, A. Zeugner, Z. S. Aliev, S. Gaß, A. U. B. Wolter, A. V. Koroleva, A. M. Shikin, M. Blanco-Rey, M. Hoffmann, I. P. Rusinov, A. Y. Vyazovskaya, S. V. Eremeev, Y. M. Koroteev, V. M. Kuznetsov, F. Freyse, J. Sánchez-Barriga, I. R. Amiraslanov, M. B. Babanly, N. T. Mamedov, N. A. Abdullayev, V. N. Zverev, A. Alfonsov, V. Kataev, B. Büchner, E. F. Schwier, S. Kumar, A. Kimura, L. Petaccia, G. Di Santo, R. C. Vidal, S. Schatz, K. Kißner, M. Ünzelmann, C. H. Min, S. Moser, T. R. F. Peixoto, F. Reinert, A. Ernst, P. M. Echenique, A. Isaeva, and E. V. Chulkov, Nature (London) **576**, 416 (2019).

[32] Y. J. Chen, L. X. Xu, J. H. Li, Y. W. Li, H. Y. Wang, C. F. Zhang, H. Li, Y. Wu, A. J. Liang, C. Chen, S. W. Jung, C. Cacho, Y. H. Mao, S. Liu, M. X. Wang, Y. F. Guo, Y. Xu, Z. K. Liu, L. X. Yang, and Y. L. Chen, Phys. Rev. X **9**, 041040 (2019).

[33] H. Li, S.-Y. Gao, S.-F. Duan, Y.-F. Xu, K.-J. Zhu, S.-J. Tian, J.-C. Gao, W.-H. Fan, Z.-C. Rao, J.-R. Huang, J.-J. Li, D.-Y. Yan, Z.-T. Liu, W.-L. Liu, Y.-B. Huang, Y.-L. Li, Y. Liu, G.-B. Zhang, P. Zhang, T. Kondo, S. Shin, H.-C. Lei, Y.-G. Shi, W.-T. Zhang, H.-M. Weng, T. Qian, and H. Ding, Phys. Rev. X **9**, 041039 (2019).

[34] Y.-J. Hao, P. Liu, Y. Feng, X.-M. Ma, E. F. Schwier, M. Arita, S. Kumar, C. Hu, R. Lu, M. Zeng, Y. Wang, Z. Hao, H.-Y. Sun, K. Zhang, J. Mei, N. Ni, L. Wu, K. Shimada, C. Chen, Q. Liu, and C. Liu, Phys. Rev. X **9**, 041038 (2019).

[35] C. Hu, K. N. Gordon, P. Liu, J. Liu, X. Zhou, P. Hao, D. Narayan, E. Emmanouilidou, H. Sun, Y. Liu, H. Brawer, A. P. Ramirez, L. Ding, H. Cao, Q. Liu, D. Dessau, and N. Ni, Nat. Commun. **11**, 97 (2020).

[36] M. M. Hosen, G. Dhakal, K. Dimitri, P. Maldonado, A. Aperis, F. Kabir, C. Sims, P. Riseborough, P. M. Oppeneer, D. Kaczorowski, T. Durakiewicz, and M. Neupane, Sci. Rep. **8**, 13283 (2018).

[37] I. Belopolski, K. Manna, D. S. Sanchez, G. Chang, B. Ernst, J. Yin, S. S. Zhang, T. Cochran, N. Shumiya, H. Zheng, B. Singh, G. Bian, D. Multer, M. Litskevich, X. Zhou, S.-M. Huang, B. Wang, T.-R. Chang, S.-Y. Xu, A. Bansil, C. Felser, H. Lin, and M. Z. Hasan, Science **365**, 1278 (2019).

[38] D. F. Liu, A. J. Liang, E. K. Liu, Q. N. Xu, Y. W. Li, C. Chen, D. Pei, W. J. Shi, S. K. Mo, P. Dudin, T. Kim, C. Cacho, G. Li, Y. Sun, L. X. Yang, Z. K. Liu, S. S. P. Parkin, C. Felser, and Y. L. Chen, Science **365**, 1282 (2019).

[39] X. Gui, I. Pletikosic, H. Cao, H.-J. Tien, X. Xu, R. Zhong, G. Wang, T.-R. Chang, S. Jia, T. Valla, W. Xie, and R. J. Cava, ACS Cent. Sci. **5**, 900 (2019).

[40] Y. Tokura, K. Yasuda, and A. Tsukazaki, Nat. Rev. Phys. **1**, 126 (2019).

[41] P. F. S. Rosa, C. Adriano, T. M. Garitezi, R. A. Ribeiro, Z. Fisk, and P. G. Pagliuso, Phys. Rev. B **86**, 094408 (2012).

[42] See Supplemental Material at http://link.aps.org/supplemental/10.1103/PhysRevB.102.165153 to this article which consists references [43–45,50–53].

[43] W. Kohn and L. J. Sham, Phys. Rev. **140**, A1133 (1965).

[44] G. Kresse and J. Furthmüller, Phys. Rev. B **54**, 11169 (1996).

[45] G. Kresse and D. Joubert, Phys. Rev. B **59**, 1758 (1999).

[46] A. M. Goforth, P. Klavins, J. C. Fettinger, and S. M. Kauzlarich, Inorg. Chem. **47**, 11048 (2008).

[47] A. M. Turner, Y. Zhang, R. S. K. Mong, and A. Vishwanath, Phys. Rev. B **85**, 165120 (2012).

[48] S. Ono and H. Watanabe, Phys. Rev. B **98**, 115150 (2018).

[49] H. Watanabe, H. C. Po, and A. Vishwanath, Sci. Adv. **4**, eaat8685 (2018).

[50] J. P. Perdew, K. Burke, and M. Ernzerhof, Phys. Rev. Lett. **77**, 3865 (1996).

[51] S. L. Dudarev, G. A. Botton, S. Y. Savrasov, C. J. Humphreys, and A. P. Sutton, Phys. Rev. B **57**, 1505 (1998).

[52] N. Marzari and D. Vanderbilt, Phys. Rev. B **56**, 12847 (1997).

[53] Q. S. Wu, S. N. Zhang, H. F. Song, M. Troyera, and A. A. Soluyanov, Comput. Phys. Commun. **224**, 405 (2018).